SPALLATION NEUTRON MEASUREMENT AT INCIDENT PROTON ENERGIES OF 0.8 TO 3 GEV

T.NAKAMOTO, K.ISHIBASHI, N.MATSUFUJI, K.MAEHATA, Y.WAKUTA,
Department of Nuclear Engineering, Kyushu University
Hakozaki, Fukuoka 812, Japan
M. NUMAJIRI
National Laboratory for High Energy Physics (KEK)
Oho, Tsukuba 305, Japan
H. TAKADA, S. MEIGO and S. CHIBA
Japan Atomic Energy Research Institute (JAERI)
Tokai-mura, Ibaraki 319-11, Japan
Y. WATANABE
Energy Conversion Engineering, Kyushu University
Kasuga-koen, Kasuga 816, Japan
T. NAKAMURA
Cyclotron and Radioisotope Center, Tohoku University
Aoba, Sendai 980, Japan
M. ARAI
Department of Physics, Kobe University
Rokkoudai, Kobe 657, Japan

ABSTRACT

It has been experimentally confirmed that the high-energy nucleon(proton or neutron) spectra from the nuclear spallation reaction are in good agreement with the results of the cascade calculation. However, low-energy nucleon spectra below several 10 MeV have not been measured for the spallation reaction for incident protons of GeV range. The experiment on the neutron-emission double-differential cross section was carried out at proton energies of 0.8, 1.5 and 3 GeV at KEK. The neutrons were measured by the time-of-flight method with a typical flight path of 1 m. The experiment for C and Pb targets was completed last November. Neutrons having energies of 1 to 300 MeV were successfully measured with acceptable uncertainty. Measurements will be continued this year to cover a few targets between C and Pb.

I. INTRODUCTION

It is of interest to investigate the neutron-emission cross section for the reaction (p,xn) by incident protons in the medium energy region. The data are useful for studying such facilities as the spallation neutron sources and the accelerator-driven transmutation systems. The experimental data were obtained by the time-of-flight (TOF) method at IUCF[1] with incident proton energies of 120 and 160 MeV, at PSI (SIN)[2] with that of 585 MeV, and at LANL[3-6] with those of 113 to 800 MeV. At higher energies than these, a test measurement[7] was made at National Laboratory for High Energy Physics (KEK). However, systematic data covering many targets have not been taken in the energy region above 800 MeV so far.

With increasing proton energy from 113 to 800 MeV, the experimental neutron cross section showed a systematic difference[5] from the calculated results in the evaporation and/or preequilibrium region. In the GeV region of incident proton energy, it is well known that the high-energy nucleon (proton or neutron) spectra from the nuclear reaction are in good agreement with the results of the cascade model calculation. A special interest attaches to the spallation neutrons with energies of 1 to 100 MeV. We have planned to measure the double differential cross section (DDX) of the spallation neutrons by the TOF method. The incident proton energies were chosen to be 0.8, 1.5 and 3 GeV. Protons were supplied by $\pi 2$ beam line at KEK. The protons are obtained as secondary particles generated by an internal target, which is placed in the accelerator ring of the 12 GeV proton synchrotron. Before performing the experiment for the cross sections, we made a preliminary measurement to check the experimental methods.

II. PRELIMINARY MEASUREMENT

Some test measurements were made at the π2 beam line with protons of 1.5 GeV. The scintillator NE213 was chosen for the neutron detection. An early question was whether or not to shield neutron detectors from background neutrons and gamma rays. The results at 90° are plotted in Fig. 1. Open triangular marks show the data taken by a bare neutron detector, while solid square ones indicate those by the detector surrounded with iron blocks of 0.5 to 1 m thick. A large disagreement is seen at a few MeV. The heavy shielding was not appropriate in the experimental circumstances. Neutron detectors were, therefore, determined to be used on the bare condition.

At first, we followed the zero-cross method[8] for the pulse-shape discrimination between neutron and gamma ray. The results by this method ware shown in Fig. 2. The discrimination was worse for high-energy events. This is because the saturation effect was induced on the zero-cross time in a pulse-shaping preamplifier, due to the very large energy-range of the incident particles. To eliminate such saturation, a two-gate integration method[9] was tested at a later test run. The photomultiplier signal was branched into two pulses, and they were input into charge ADCs worked by different gate pulses. The fast gate on one ADC covered the initial peak of the photomultiplier signal, whereas the tail gate made another ADC to accept the slow-tail portion thereof. The fast gate had a duration of 30 ns, and the tail gate owned that of 500 ns after a delay of 130 ns. The results are shown in Fig. 3. The discrimination is excellent and the above saturation effect is not seen. The two-gate integration method was adopted in the measurement thereafter.

The simplest method for background correction is to make two kinds of experiments of target-in and -out measurements: The cross section is obtained by subtracting the latter data from the former ones. However, in this case, the influence from such effects as the floor-scattered (or -generated) neutrons may not be removed. We were afraid that the floor-scattering effect might arise because of the rather short height (1.7 m) between the floor and the beam line. The experimental check was made by inserting a shadow bar of 1 m length between target and detector. The detector was placed at the beam -line level with a TOF flight path of 1.5 m. The results at 60 deg are shown in Fig. 4, together with the cross section measured. One can see the effect like the floor scattering is negligible in the energy region at the flight path.

III. EXPERIMENTAL ARRANGEMENTS

The experimental specification is listed in Table 1. The NE213 detectors have two kinds of sizes (Φ5"×5" and Φ2"×2"). The larger detectors were used for making the neutron-detection efficiency as high as possible, although they produce a rather poor time resolution in the TOF measurement. The smaller ones exhibit good neutron-gamma pulse-shape discrimination even in the neutron energy region around 1 MeV.

The experimental arrangement is illustrated in Fig. 5. The beam intensity of the π2 beam was very weak and in a level of 10^5 particles/2.5s because of its generation as a secondary beam. Incident particles were counted one by one by plastic scintillators. The protons were identified from pions by a pair of TOF scintillators (Pilot U) located at a separation distance of 20 m. Each Pilot U scintillator was connected on opposite sides with two photomultipliers (Hamamatsu H2431). The particle identification is shown in Fig. 6, for instance, at a beam momentum of 3.83 GeV/c, i.e. proton kinetic energy of 3.0 GeV. The time signals of the two sides were averaged by software. The time resolution was 0.35 ns, and protons are well discerned from pions having a separation time of 1.7 ns.

For the neutron TOF measurement, the time standard was taken by the Pilot U scintillator adjacent to the target. The beam-incident target area was defined by a pair of scintillators. Because of the low beam intensity, the flight path of the neutron TOF was limited to short distances: It was 1 to 1.5 m for the Φ5"×5" detectors, and 0.6 to 0.9 m for Φ2"×2" ones. The values of flight path were shorter than the beam-line height 1.7 m from the floor. Veto plastic scintillators were used for finding charged-particle events in the neutron detectors. They were installed in front of all neutron detectors as illustrated in Fig. 5. The picture of the detector system is presented in Fig. 7. The whole frame was made of aluminum alloy. The 5" detectors were arranged over the beam line, for the redundant safety for the floor-scattering effect. The beam damp was formed by carbon of 0.5×0.5 m^2 in area and 1 m thick. The carbon

was surrounded by sufficiently thick iron blocks except at the beam-incident surface. The distance between the target and the beam dump was 8.5 m.

The block diagram of the measurement circuit is shown in Fig. 8 with simplified drawing. When the incident-beam coincidence took place at all the beam scintillators, the pulse with a typical width of 150 ns was sent to the next coincidence module. Then, the signal of neutron detectors was accepted by this module for 150 ns. The events arising from incident pions were eliminated by tuning a hardware timing in the beam coincidence. The example of the TOF spectrum is shown in Fig. 9. The prompt gamma rays are seen as a sharp peak in the right hand side. The time resolution of the neutron TOF measurement was 0.96 ns for 5" detectors and 0.55 ns for 2" ones.

The detection efficiency of the neutron detectors was calculated by the use of the Cecil code[10] of the Kent State University version. The experimental check on the detection efficiency has recently performed at JAERI for neutrons with energies below 30 MeV. Although detailed analysis for the experiment was not made completely, we considered that the experimental efficiency was close to or slightly (~10%) below the calculated values. In this paper, the detection efficiency as calculated is utilized for converting the measured TOF events into the cross sections.

IV. EXPERIMENTAL RESULTS

The measurement has already been carried out for targets of Pb and C at proton energies of 0.8, 1.5 and 3.0 GeV. The preliminary DDX data are shown in Figs. 10-12 for Pb and Figs. 13-15 for C. The relatively worse time resolution for the short flight path lead to considerable ambiguity in neutron energies above 200 MeV as listed in Table 2; we are not concerned about it because our interest is mainly in the evaporation (and preequilibrium) neutrons. Calculation results by the cascade-evaporation model (HETC)[11] was shown by lines. The experimental data at 0.8 GeV are compared with those[5,6] of LANL in Fig. 16. The present preliminary DDX agrees with the LANL data typically within a discrepancy of 10%. Further checks and corrections will be made on such items as the detection efficiency and multiple scattering effects in the target itself. The measurements for other targets i.e. Al, Fe, and In are to be performed in 1993.

The measurement data are converted into a linear scale on the vertical axis: The cross section are plotted with normalization by $\ln(E_{n+1})-\ln(E_n)$ instead of conventional method of $E_{n+1}-E_n$. The linearized data are shown in Figs. 17 and 18 for proton energies of 0.8 and 3.0 GeV, respectively. The calculated values of the evaporation component are clearly higher than the experimental data in Fig.18 for 3.0 GeV protons, but such difference is not seen in Fig.17 for 0.8 GeV. The overestimation in the evaporation region in Fig.18 may be attributed to the lack of theoretical consideration on the fragmentation phenomenon, which appears at high incident energies around 3 GeV.

V. CONCLUSION

The measurement of (p,xn) reaction at incident proton energies of 0.8, 1.5 and 3.0 GeV was started. The experimental difficulties were overcome through the test measurement. The measurement on the heaviest element of Pb and the lightest C had already been carried out. The DDX for Pb at 0.8 GeV was compared preliminarily with the LANL data, and was confirmed to agree with them in an acceptable manner. Further experiment on the rest of the targets is planned to be completed in 1993.

The authors express their gratitude to Prof. K. Nakai and the beam channel staffs of KEK for his continuous encouragement and their generous support of this experiment, and tender their acknowledgements to Prof. H. Hirabayashi and Prof. N. Watanabe of KEK, and Prof. M. Arai of Kobe University for their useful discussion.

REFERENCES

1) W.Scobel et al.: Phys. Rev. C 41 (1990) 2010.
2) S.Cierjacks et al.: Phys. Rev. C 36 (1987) 1976.

3) M.Meier et al.: Radiation Effects 196 (1987) 1415.
4) M.Meier et al.: Nucl.Sci.Eng. 104 (1990) 339.
5) W.Amian et al.: Proc. Nucl. Data for Sci. and Technol. (1991) p.696
6) W.Amian et al.: Nucl.Sci.Eng. 112 (1992) 78.
7) R.Chiba: Genshikaku-kenkyu 21 (1985) 41 in Japanese.
8) P.Plischke et al.: Nucl. Instrum. Meth. 139 (1976) 579.
9) Z.W.Bell et. al.: Nucl. Instrum. Meth. 188 (1981) 105.
10) R.A.Cecil et al.: Nucl. Instrum. Meth. 161 (1979) 439.
11) F.Atchison : JUL-CONF-34 (1980)

Table 1 Experimental specification

Proton energy (GeV)	0.8, 1.5, 3.0
Targets (thickness)	C(10cm), Pb(1.2cm) Al, Fe, In (planned)
Method	Time of Flight
Neutron detector	NE213, Φ2"×2" and Φ5"×5"
Flight path (m)	0.6~0.9 for Φ2"×2"
	1~1.5 for Φ5"×5"
Photomuliplier	H1250 for Φ5"×5"
	H1161 for Φ2"×2"
	H2431 for Pilot-U
Angle (deg)	15, 30, 60, 90, 120, 150

Table 2 Neutron energy resolution*

Neutron energy(MeV)	Flight time(ns)	Energy resolu.(%)
3	46	5.5
10	25	5.8
30	15	7.5
100	8.6	12
200	6.5	18
300	5.6	23
400	5.1	28

*TOF with a mean flight path of 1.1m and a time resolution of 0.96 ns.

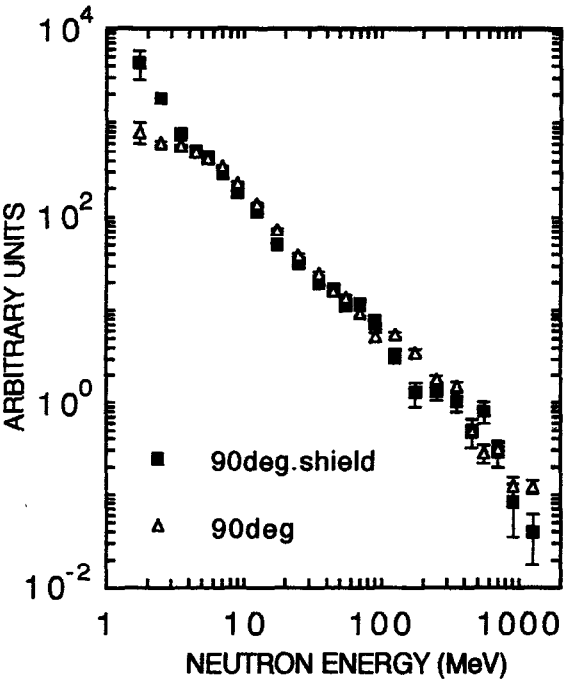

Fig. 1 Neutron spectra at 90° by 1.5 GeV protons with and without iron shielding around a neutron detector. The vertical axis is in a relative scale.

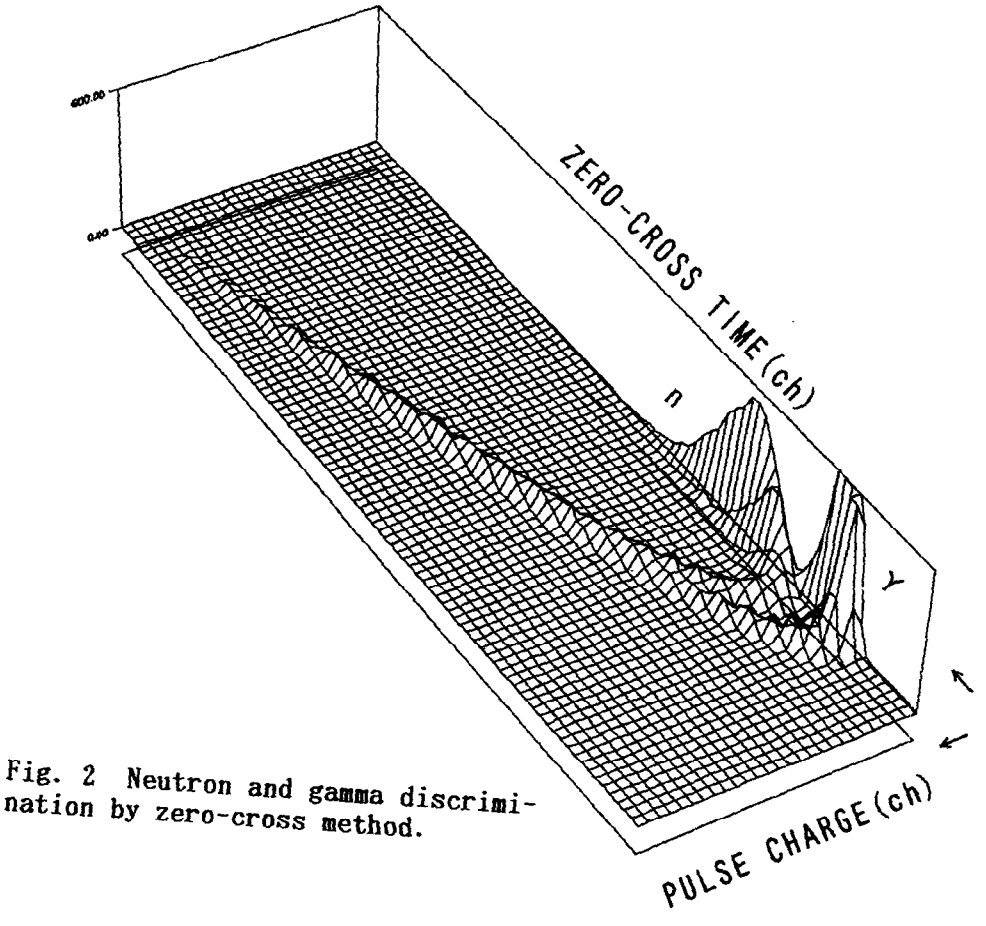

Fig. 2 Neutron and gamma discrimination by zero-cross method.

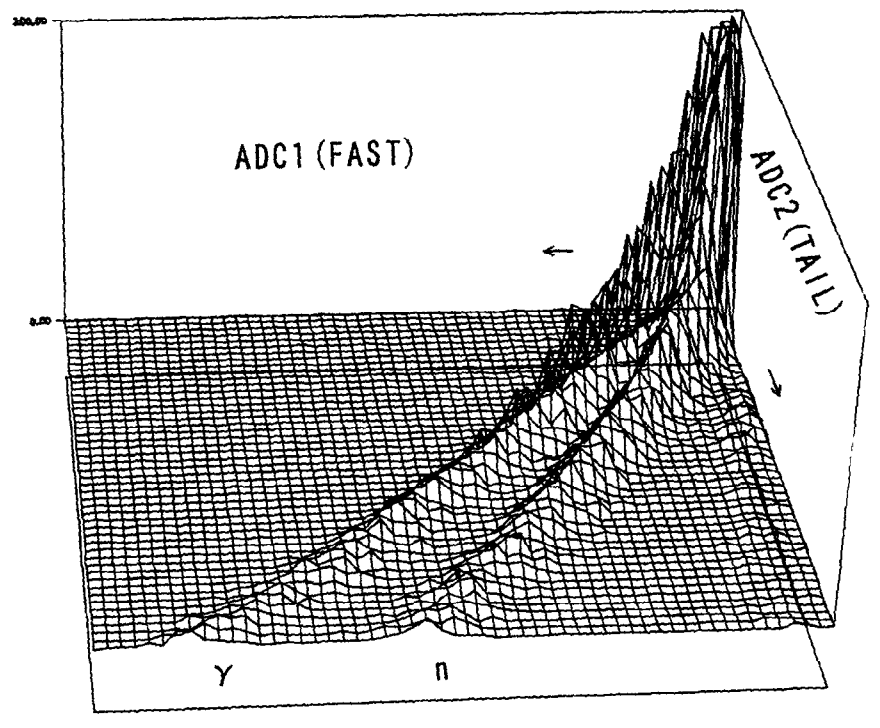

Fig. 3 Neutron and gamma discrimination by two-gate integration method.

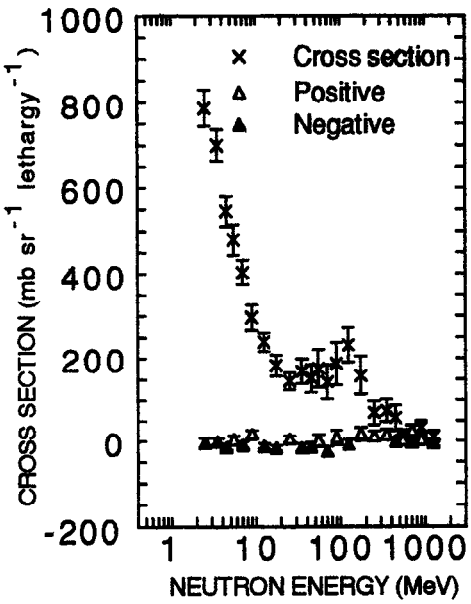

Fig. 4 Results of the shadow bar test. The shadow bar size was ϕ15x 100cm^2 and the flight path 1.5 m. The vertical axis is linearized by the use of lethargy $\ln(E_{n+1})-\ln(E_n)$.

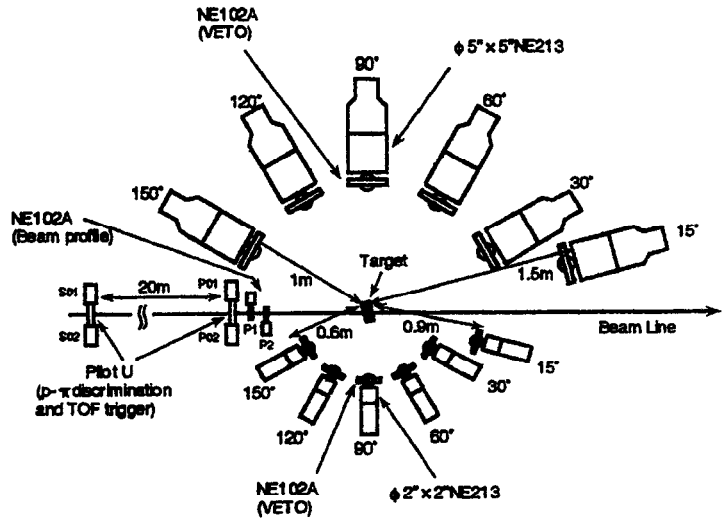

Fig. 5 Illustration of the experimental arrangement.

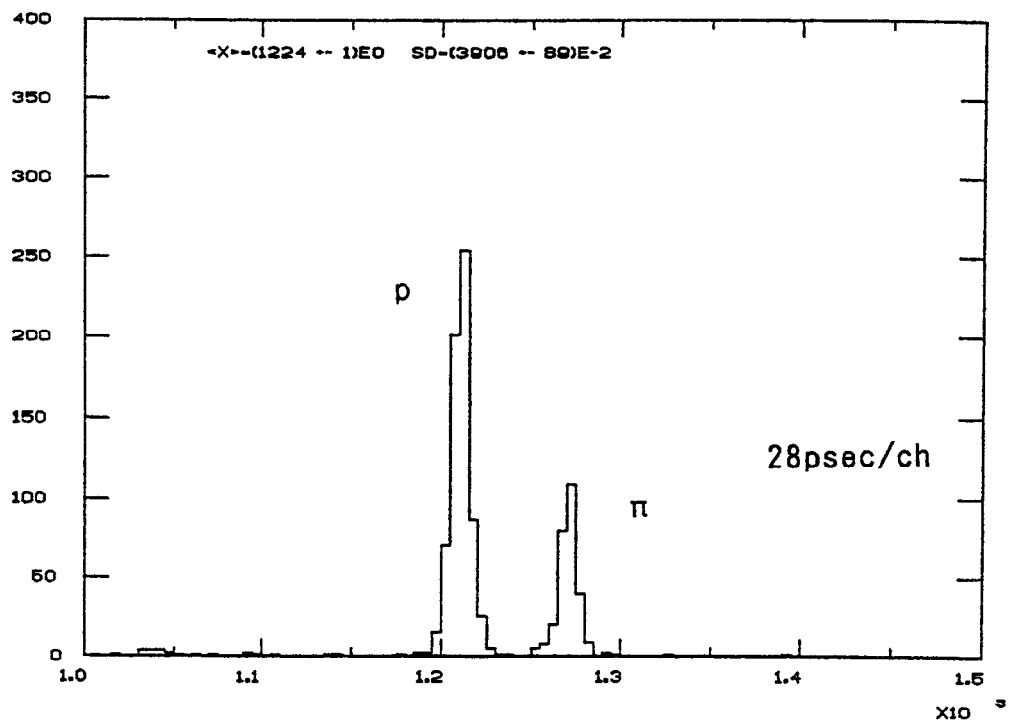

Fig. 6 Proton-pion separation in TOF spectrum for beam of 3.83 GeV/c.

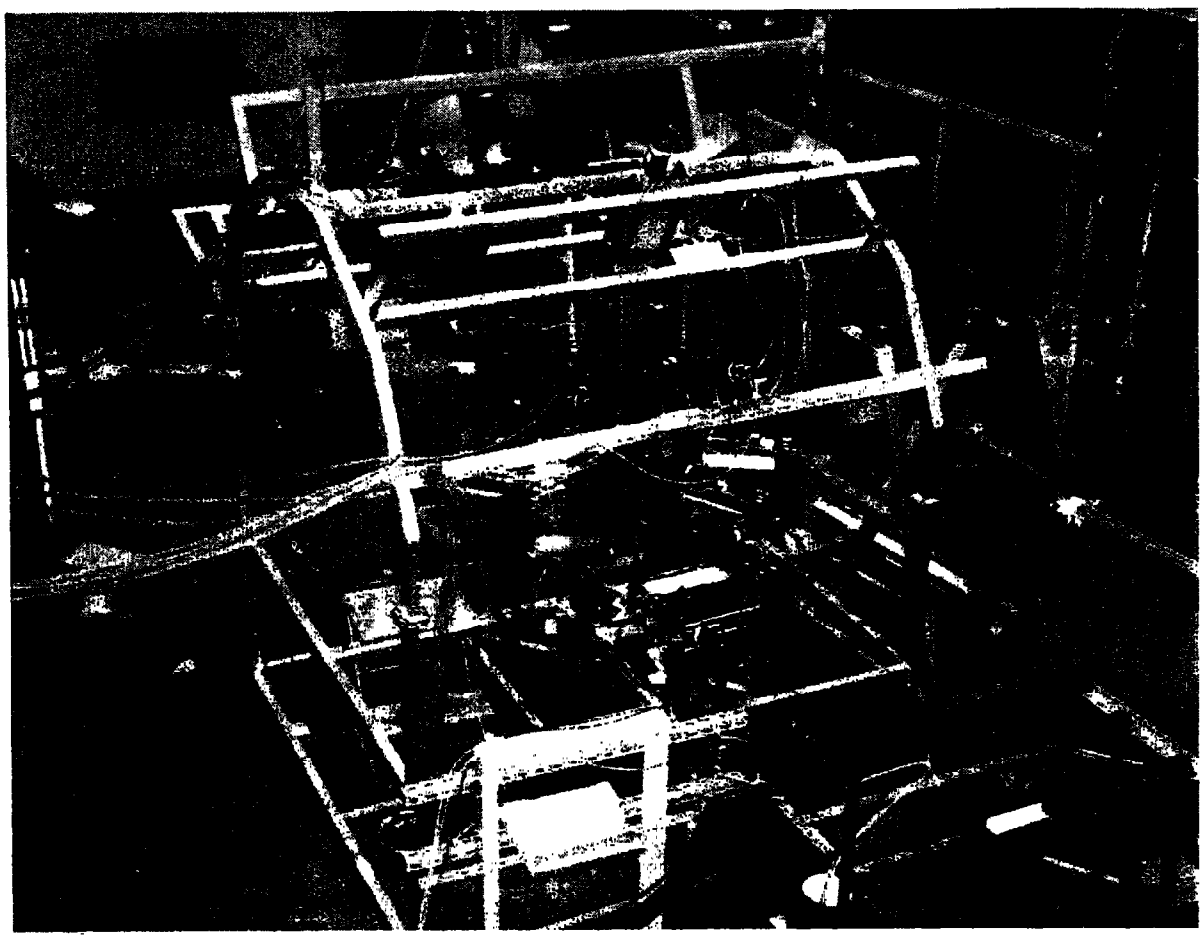

Fig. 7 Picture of the detector system. Incident particles come from the right side.

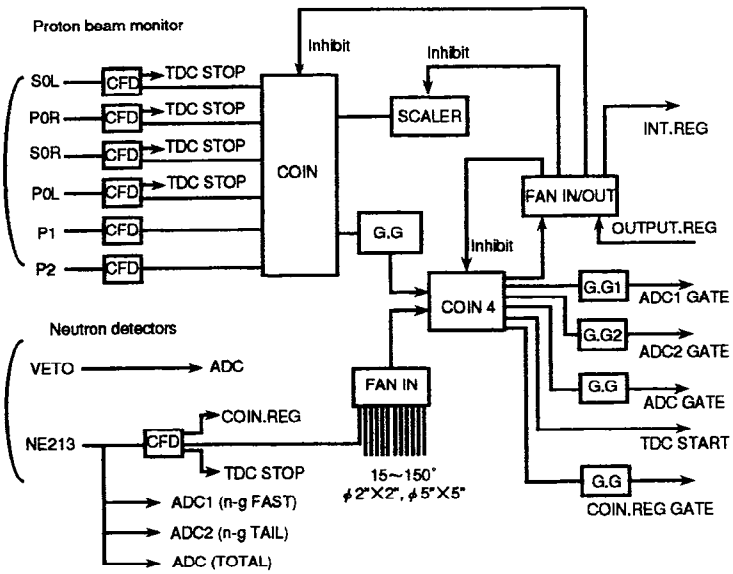

Fig. 8 Block diagram of the electronic system with simplification.

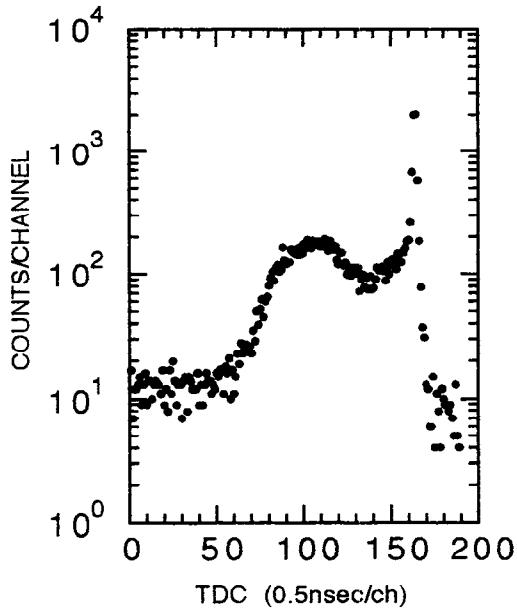

Fig. 9 TOF spectrum at 15° for an incident proton energy of 1.5 GeV.

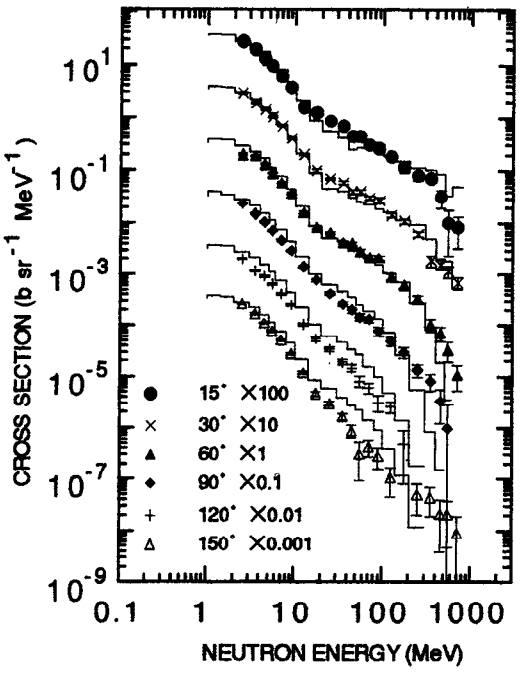

Fig.10 Double differential cross section at 0.8 GeV for Pb. Lines show calculation results by HETC.

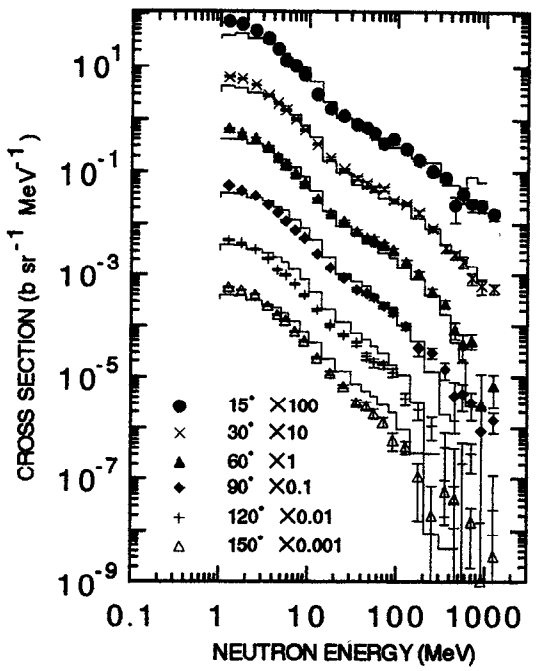

Fig.11 Double differential cross section at 1.5 GeV for Pb. Lines show calculation results by HETC.

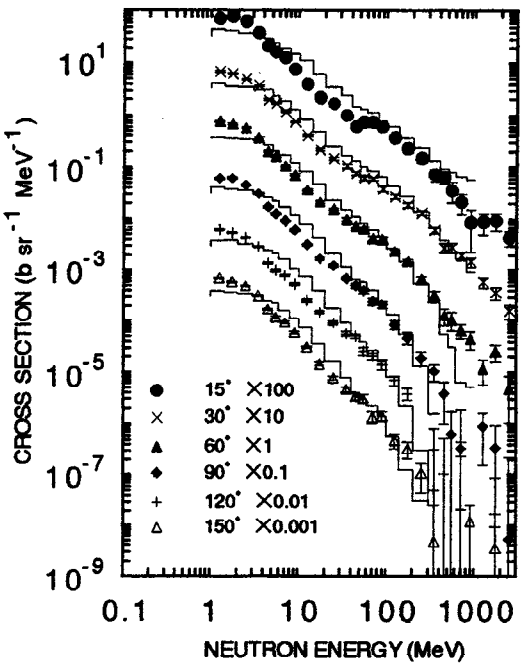

Fig.12 Double differential cross section at 3.0 GeV for Pb. Lines show calculation results by HETC.

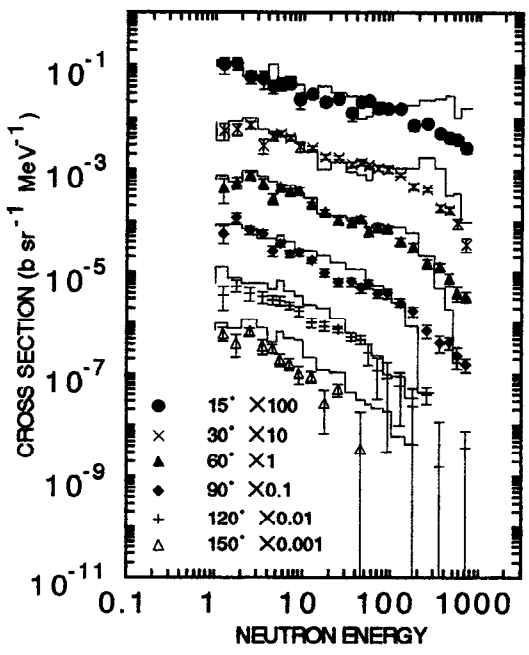

Fig.13 Double differential cross section at 0.8 GeV for C. Lines show calculation results by HETC.

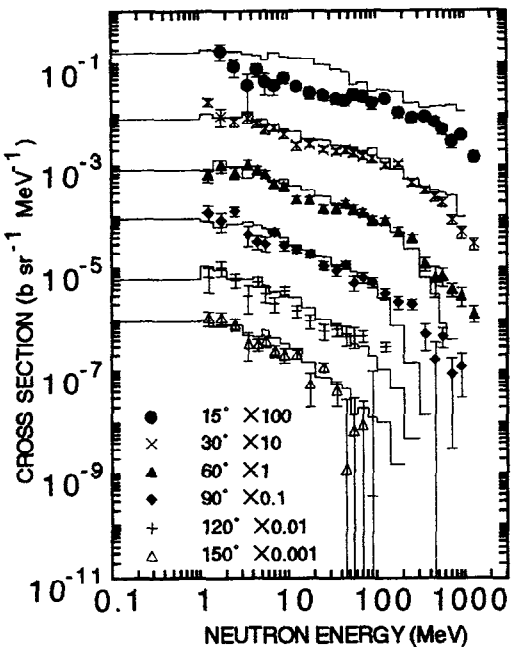

Fig.14 Double differential cross section at 1.5 GeV for C. Lines show calculation results by HETC.

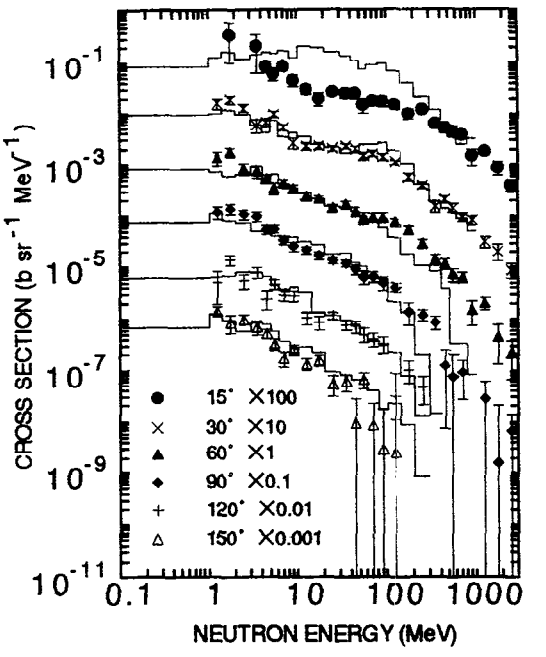

Fig.15 Double differential cross section at 3.0 GeV for C. Lines show calculation results by HETC.

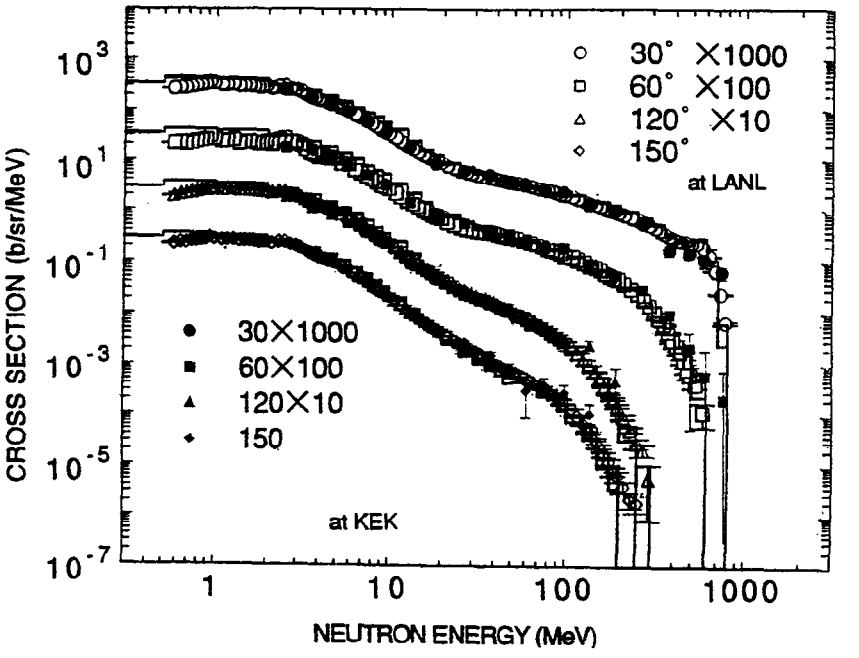

Fig.16 Double differential cross section at 0.8 GeV for Pb, presented together with the results of LANL.

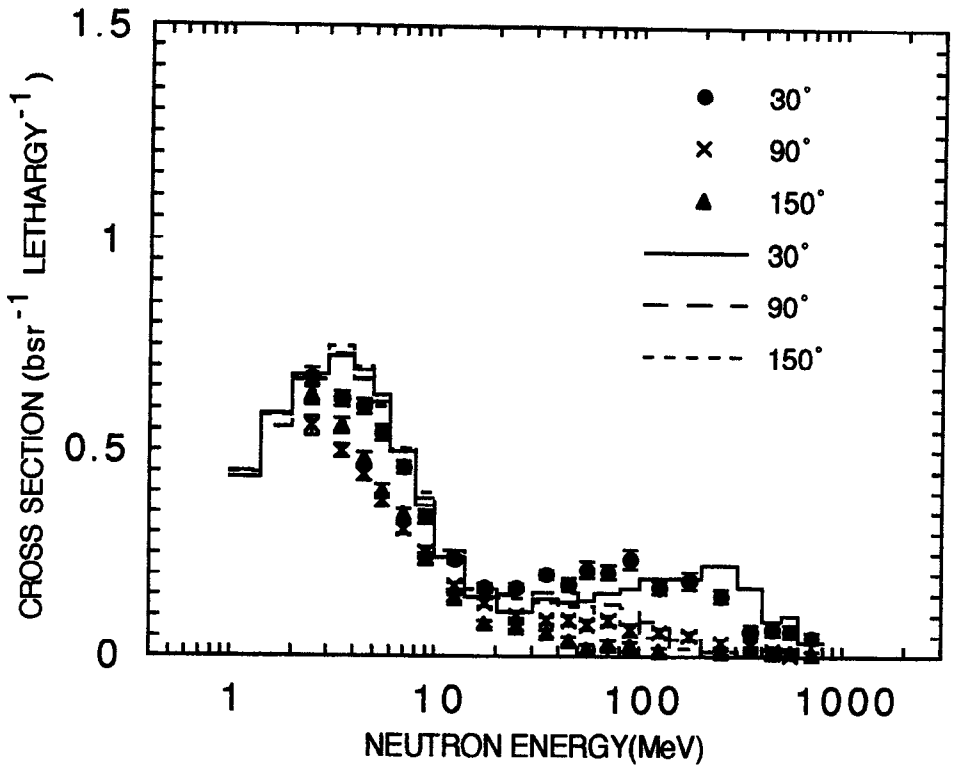

Fig.17 Linearized cross sections at 0.8 GeV for Pb. Lines show the results of HETC calculation. The lethargy of $\ln(E_{n+1})-\ln(E_n)$ is used for the vertical axis.

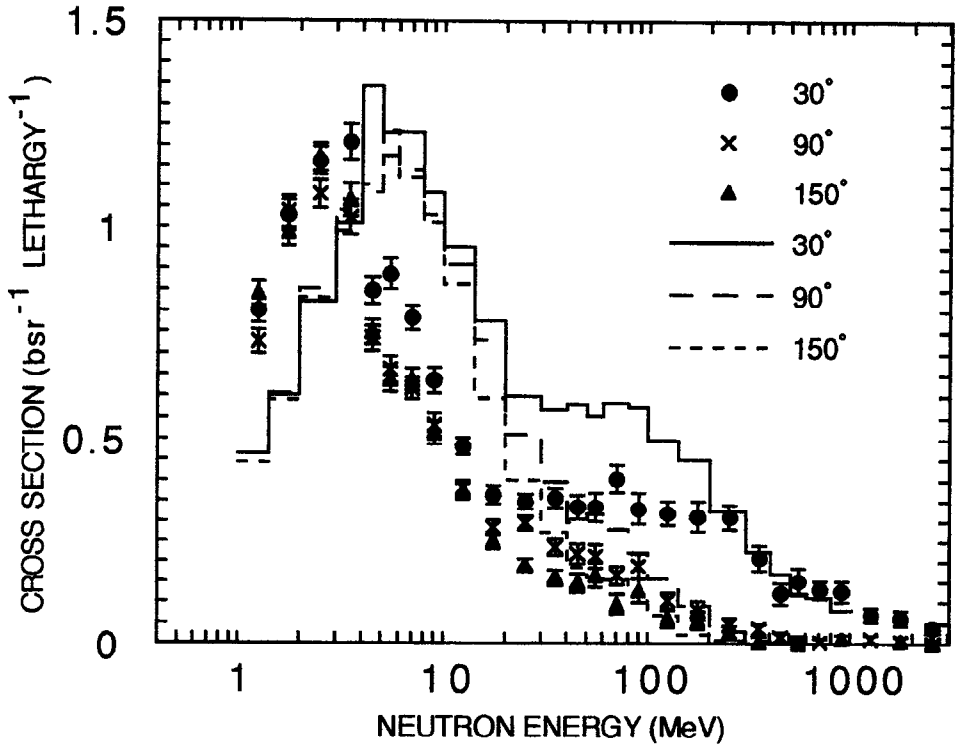

Fig.18 Linearized cross sections at 3.0 GeV for Pb. Lines show the results of HETC calculation. The lethargy of $\ln(E_{n+1})-\ln(E_n)$ is used for the vertical axis.